

Thermal dark matter via the flavon portal

Carlos Alvarado,^{*} Fatemeh Elahi,[†] and Nirmal Raj[‡]

*Department of Physics, University of Notre Dame,
225 Nieuwland Hall, Notre Dame, Indiana 46556, USA*

Dark matter (DM) is added to the Froggatt-Nielsen (FN) mechanism, and conditions for its successful freezeout identified. Requesting the FN scale Λ_{FN} to be the cutoff of the theory renders freezeout scenarios surprisingly few. Fermionic DM is typically charged under $U(1)_{\text{FN}}$, with the dominant annihilation channel a CP-even flavon + CP-odd flavon. A minimal case is when the DM-flavon coupling strength is $\mathcal{O}(1)$, with several implications: (1) the DM mass is $\mathcal{O}(100 \text{ GeV} - 1 \text{ TeV})$, thanks to the WIMP coincidence, (2) requiring perturbativity of couplings puts a lower *and* upper limit on the flavor scale, $2 \text{ TeV} \lesssim \Lambda_{\text{FN}} \lesssim 14 \text{ TeV}$, on account of its relation to DM mass and couplings, (3) DM is a “secluded WIMP” effectively hidden from collider and direct detection searches. Limits on the masses of dark matter and mediators from kaon mixing measurements constitute the best constraints, surpassing Xenon1T, Fermi-LAT, and the LHC. Future direct detection searches, and collider searches for missing energy plus a single jet/bottom/top, are promising avenues for discovery.

I. INTRODUCTION

The nature and origin of dark matter (DM) remain elusive. Since the Standard Model (SM) does not account for a DM candidate, it is natural to seek one in extensions of it devised to confront its other problems. This approach enjoys an obvious merit: a single theory can account for (at least) two problems. Thus, solutions to the electroweak (EW) hierarchy problem (e.g. weak scale supersymmetry and little Higgs) provide DM when a “new physics” parity is imposed, right-handed neutrinos introduced to explain small neutrino masses, or axions introduced by the Peccei-Quinn resolution to the strong CP problem, may serve as DM – and so on. Can DM be addressed in the problem of fermion flavors?

Fermion masses are hierarchical across many orders, and mix in peculiar patterns. That these may be accidents of nature is an explanation we find unsatisfactory. A simple alternative may be found in the mechanism of Froggatt and Nielsen (FN) [1], that extends the SM gauge group with a (global or local) symmetry. The lightness of fermions f is then arranged by mixing with heavy fermions F vector-like under the new and SM symmetries: $SFf + \Lambda_{\text{FN}}F\bar{F}$, where S is the “flavon”, a scalar field acquiring a vev v_s and breaking the symmetry. The SM Yukawa matrices are now nothing but powers of $\epsilon \equiv \langle S \rangle / \Lambda_{\text{FN}}$ in an effective field theory (EFT), with ϵ usually fixed to the Cabibbo angle $\simeq 0.23$. Both the mass and mixing hierarchies can be obtained now, but flavor changing neutral currents (FCNCs) are in-

evitable. To avoid constraints from FCNCs, it is found that $\Lambda_{\text{FN}} > 2 \text{ TeV}$ [2].

It is to this picture that we wish to add DM. A profitable pursuit, one that gives experiments a well-motivated target, is to identify the class of parameters that results in the correct relic abundance through $2 \rightarrow 2$ annihilations, in the spirit of such multi-parameter DM frameworks as supersymmetric neutralinos [3–5], minimal DM [6, 7], secluded WIMPs [8], effective WIMPs [9, 10], and forbidden DM [11, 12]. In other words, our first goal is to locate the “relic surface”. Our other guiding principle is to add no more than a minimal set of mass scales to the FN mechanism. To begin with, we are not interested in the case of DM annihilations to the vector-like F 's, as this puts DM mass $> \Lambda_{\text{FN}}$ and generally out of current reach. Thus, through operators suppressed by suitable powers of Λ_{FN} , DM must annihilate to SM fields and the flavon quanta that are obtained by expanding S around its vev,

$$S = \frac{1}{\sqrt{2}}(v_s + \sigma + i\rho) . \quad (1)$$

Λ_{FN} is now the “messenger scale” for DM interactions with SM and S , or in other words, the cutoff of our theory. Following the FN procedure, we will arrange our EFT interactions by populating this scale with additional vector-like fermions. One can broadly see where this leads if DM is a fermion singlet χ . Assuming it to be odd under a Z_2 symmetry in order to avoid the operator $LH\chi$, one may find that interactions with all SM species must be suppressed by negative powers of Λ_{FN} , sometimes with extra suppression from factors of v/Λ_{FN} (where v is the Higgs vev) as well as from powers of ϵ (determined by the FN charges of SM and χ). It can be verified – and we will explicitly show it – that these effects cause $\chi\bar{\chi} \rightarrow \text{SM SM}$

^{*} calvara1@nd.edu

[†] elahif7@gmail.com

[‡] nraj@nd.edu

to be too feeble, with the cross section $\langle\sigma v\rangle$ many orders smaller than $(\eta) 2.2 \times 10^{-26} \text{ cm}^3 \text{ s}^{-1}$ (where $\eta = 1$) (2) for Majorana (Dirac) DM) that is required for the correct abundance. DM interactions with the flavon, on the other hand, *need not* be Λ_{FN} -suppressed and may be arranged with marginal operators, as we shall show in this work. Couplings of $\mathcal{O}(0.1 - 1)$ are easily arranged, rendering annihilations to the flavon particles σ and ρ a viable avenue. Thus χ can be a “secluded WIMP” [8, 13]: it achieves the correct relic density by annihilating primarily to mediators (here σ and ρ), while keeping direct couplings to SM small. In this first paper, we will focus on a scenario where χ is charged under the flavor symmetry and interacts with the flavon through a renormalizable Yukawa term $y_{\text{DM}}\chi\chi S$; the best constraints on this species of secluded WIMP come from indirect limits imposed by flavor experiments. In a follow-up paper [14], we will extend our findings to cases where DM-flavon interactions are non-renormalizable, identify parametric families that lead to correct freezeout (while including SM annihilation channels that may become important), and derive all relevant constraints.

A most remarkable feature here is the hand played by the non-zero flavor charge of DM. Due to this charge, DM mass must stem from symmetry-breaking as $\propto v_s \sim \epsilon\Lambda_{\text{FN}}$. And parametrically, the cross section of χ ’s annihilation to the flavon mediators is given by $\langle\sigma v\rangle \sim y_{\text{DM}}^4/m_\chi^2$. Since perturbative unitarity limits m_χ from above [15], an *upper* limit on Λ_{FN} is imposed. As a result, lower limits on Λ_{FN} which may be placed by future flavor experiments or high-energy collider searches can potentially falsify our premise. Moreover, since perturbativity at the flavor scale restricts y_{DM} to be $\mathcal{O}(1)$, we know from the lore of the “WIMP miracle” that, to obtain the characteristic $\langle\sigma v\rangle_{\text{th}} = (\eta) 2.2 \times 10^{-26} \text{ cm}^3 \text{ s}^{-1}$, m_χ must be $\lesssim 10$ TeV. Thus, although all the masses introduced here (Λ_{FN} , v_s , m_χ) were *a priori* free to be arbitrarily heavy, requiring correct freezeout puts them all within current experimental reach. This attribute of a low-energy flavor-breaking scale emerging from a connection between DM and flavor was pointed out in [16]. It is comparable to [17–20], where a low Λ_{FN} is obtained by breaking the flavor symmetry with electroweak Higgs doublets. See also [21] for model-independent constraints on low-scale flavor-breaking.

The above features will be spoiled if DM is a scalar, in which case it can have a renormalizable interaction with the Higgs doublet through a portal term: $|\chi|^2|H|^2$. Annihilations to the SM Higgs boson must dominate unless the coupling is tuned to be small, and there is no intimate relation between the DM abundance and the FN mechanism. For these reasons our study will only focus on fermionic DM.

A Froggatt-Nielsen portal to DM was explored in [16], but the presence of the CP-odd flavon was omitted and emphasis was not placed on obtaining the correct relic abundance. Here we will show that the CP-odd flavon plays a primary role in freeze-out. The status and prospects of the CP-odd flavon were explored in comprehensive detail in [2], whose results we will use extensively in this work. For other works that explore the interface between flavor and dark matter, see [22–34] and the references in [35].

This paper is laid out as follows. We first review the FN mechanism in Sec. II. DM is carefully incorporated into this set-up in Sec. III. We will find this a non-trivial task: we begin with a brief overview of simple models in Sec. III.1 and show them to be ineffective or unsatisfactory, before moving on to a successful model that requires χ to be charged under $U(1)_{\text{FN}}$. Sec. IV discusses constraints and future prospects, and Sec. V concludes the paper.

II. FROGGATT-NIELSEN MECHANISM

We begin with a brief review of the FN mechanism; for a more thorough review, see [36]. Ingredients relevant for embedding DM (performed in the next section) will be given emphasis. The FN mechanism introduces an array of heavy vector-like fermions of mass Λ_{FN} transforming under the SM gauge group as well as under a new symmetry that is either global, local or discrete; we will use a global $U(1)_{\text{FN}}$ for illustration. The symmetry also transforms a new complex scalar S , the flavon, and all SM fermions excepting the top quark; the Higgs doublet is neutral under it. Conventionally, S is assigned a $U(1)_{\text{FN}}$ charge -1, which we assume hereafter. The charge assignments ensure that in the theory below Λ_{FN} , fermions couple to the Higgs doublet only via non-renormalizable terms containing several powers of S (or no power in the case of the top quark):

$$\mathcal{L} \supset y_{ij}^{(u)} \left(\frac{S}{\Lambda_{\text{FN}}} \right)^{m_{ij}} \bar{Q}_i u_j \tilde{H} + y_{ij}^{(d)} \left(\frac{S}{\Lambda_{\text{FN}}} \right)^{n_{ij}} \bar{Q}_i d_j H, \quad (2)$$

where $\tilde{H} = i\sigma_2 H^*$ and the exponents m_{ij} , n_{ij} are determined by the FN charges of the fermions. For simplicity, we have assumed only quarks to be charged under the FN symmetry, though the mechanism can be easily extended to leptons as well. The $U(1)_{\text{FN}}$ symmetry breaks if S develops a vev v_s , giving rise to Yukawa couplings that are parameterically powers of $\epsilon = v_s/\sqrt{2}\Lambda_{\text{FN}}$. Thus, fermion masses and mixings originate in both electroweak symmetry breaking (EWSB) and flavor breaking, with their relative sizes set by the number of ϵ powers. The

size of ϵ is traditionally fixed by matching with measurements of the Cabibbo-Kobayashi-Maskawa (CKM) matrix: $\epsilon \simeq |V_{us}| \simeq |V_{cb}| \approx 0.23$. Once the hierarchies are fixed to the right order this way, dimensionless $\mathcal{O}(1)$ coefficients $y_{ij}^{(u,d)}$ can bring the CKM entries and fermion masses to their measured values¹.

Thus far we have described the FN mechanism without explicit reference to the flavor group at work, which can be continuous, discrete, global, local, abelian, or non-abelian. In our work we choose a global $U(1)_{\text{FN}}$ for simplicity. Symmetry-breaking must introduce a potentially troublesome Goldstone boson ρ , disfavored by cosmological constraints if it couples to the SM [37–39]. This problem is evaded if the pseudoscalar ρ acquires a non-zero mass through explicit breaking² in the potential:

$$V(H, S) = -\mu_s^2 |S|^2 + \lambda_s |S|^4 + \lambda_{sh} |S|^2 H^\dagger H - b^2 (S^2 + \text{H.c.}), \quad (3)$$

giving rise to the physical masses post-minimization

$$m_\sigma^2 = 2\lambda_s v_s^2, \quad m_\rho^2 = 4b^2, \quad (4)$$

with $b^2 > 0$ and $v \simeq 246$ GeV. Though b^2 is a free parameter, as it is the only term explicitly breaking $U(1)_{\text{FN}}$, it is multiplicatively renormalized and can be naturally smaller than the other scales here. Thus we require m_ρ to lie below Λ_{FN} and assume the mass hierarchy in Ref. [2]:

$$m_\rho < m_\sigma \simeq v_s < \Lambda_{\text{FN}}.$$

Eq. 2 determines the Yukawa couplings $(g_s)_{ij}$ of σ and ρ with quark pairs of families i and j , written out explicitly in Appendix A. These couplings generate tree-level FCNC processes, due to which the FN set-up confronts limits from measurements of meson mixing, meson decays, and top quark decays, with the strongest constraints imposed by the neutral kaon mixing CP-violation parameter ϵ_K [2]. The latter constrains the masses of σ and ρ , which can be translated to limits in $\{\lambda_s, v_s, m_\rho\}$ space³. The constraint is weak at $m_\rho \simeq m_\sigma \approx 200$ GeV due to an accidental cancellation

in the Wilson coefficients of $\Delta F = 2$ operators, but when $m_\rho \gg 200$ GeV, the contribution of the flavon quanta goes as $(g_\sigma)_{sd}^2/m_\sigma^2 \propto (\lambda_s v_s^4)^{-1}$ (from Eqs. 4 and 11). Thus a lower limit on v_s and $\Lambda_{\text{FN}} = v_s/(\sqrt{2}\epsilon)$ may be obtained if we require the coupling λ_s to be perturbative. From Ref. [2], we have

$$\begin{aligned} \lambda_s \leq 4\pi &\Rightarrow v_s \geq 670 \text{ GeV} \\ &\Rightarrow \Lambda_{\text{FN}} \geq 2.07 \text{ TeV}, \end{aligned} \quad (5)$$

which will serve for the purposes of this paper as absolute lower limits on v_s and Λ_{FN} .

Once we embed DM into the FN picture, the above constraints may also restrict DM masses. Therefore, we will revisit these constraints in more detail in Sec. IV, while in the next section we proceed to our principal task of adding DM.

III. INCORPORATING DM

III.1. General model-building

Having described the interactions of the flavon quanta $s = \sigma, \rho$ with SM states, we turn to our central program of incorporating fermionic DM into the FN setup.

The following are general considerations to keep in mind before we delve into the details of model-building.

- As mentioned in the Introduction, we impose a Z_2 symmetry under which SM fields and S are even and χ is odd. This prevents operators of the form $(S/\Lambda)^k H L \chi$ that could result in DM decay, where $k \geq 0$ is an integer.
- We also mentioned in the Introduction that annihilations to SM species are suppressed by inverse powers of the cutoff scale and ϵ , and that successful freezeout is only obtained through annihilations to the flavons. Hence our emphasis in the following will be on DM interactions with flavons. All these low-energy interactions are assumed to arise from vector-like fermions integrated out at the scale Λ_{FN} . Some of these vector-like fermions, F_χ, \bar{F}_χ , must be charged odd under the Z_2 symmetry that stabilizes DM. In principle these vector-like fermions could have arbitrary masses, but we have chosen for them a common mass Λ_{FN} in line with our objective of keeping the number of new mass scales at a minimum. Thus the theory at high scales would appear as

$$\mathcal{L} \supset S \chi \bar{F}_\chi + \Lambda_{\text{FN}} F_\chi \bar{F}_\chi.$$

¹ The y_{ij} must be complex to account for the CKM phase.

² Alternatively, $U(1)_{\text{FN}}$ may be either (i) gauged, which may however introduce anomalies as the left- and right-handed fermions are charged differently, or (ii) discretized, in which case there is no Goldstone boson. Through the Z_N -preserving operator $S^N/\Lambda_{\text{FN}}^{N-4}$, where N is the dimension of the Z_N group, one has $m_\rho^2 \sim \epsilon^{N-4} v_s^2$. Successful FN models require $N \leq 16$ since the up quark demands an ϵ^8 suppression, implying a very light ρ for $v_s \sim \mathcal{O}(\text{TeV})$ that is already excluded by flavor constraints [2].

³ Through the rest of the paper we take into account the fact that the right-hand sides of Eq. 4 are $2 \times$ those in Ref. [2]

- Annihilations of a DM pair into $\sigma + \rho$ are s -wave, whereas annihilations into $\sigma\sigma$ and $\rho\rho$ are p -wave. We see this from parity considerations. The fermion-pair initial state has $P = (-1)^{L+1}$, thus the $L = 0$ transition is allowed for the parity-odd $\sigma\rho$ final state, and forbidden for the parity-even $\sigma\sigma$ and $\rho\rho$ final states.
- As χ can in principle be either neutral or carry an (arbitrary) $U(1)_{\text{FN}}$ charge, we must seek a successful model by sifting through the possibilities.

With these considerations, we now explore the freeze-out of DM neutral or charged under $U(1)_{\text{FN}}$.

III.1.1. $U(1)_{\text{FN}}$ -neutral DM

Here DM has a bare Majorana mass m_χ , and connects to the flavon via the lowest dimension operator $\chi\chi|S|^2/\Lambda_{\text{FN}}$. Assuming CP-violating phases vanish, the interactions

$$\chi\chi\rho^2/\Lambda_{\text{FN}}, \quad \chi\chi\sigma^2/\Lambda_{\text{FN}}, \quad \epsilon\chi\chi\sigma$$

are obtained from Eq. 1. These give rise to the annihilation of χ to pairs of σ and ρ , which are p -wave-suppressed. In addition, annihilation through the first two is Λ_{FN} -suppressed, and that through the third is non-trivial to arrange: χ must be heavier than σ to kinematically allow it, and at least an order of magnitude lighter than Λ_{FN} for the EFT to be valid. From Eq. 4, this means $v_s < m_\chi \ll \Lambda_{\text{FN}}$ for the quartic coupling $\lambda_s \sim 1$. However, this is not possible since $v_s \simeq \epsilon\Lambda_{\text{FN}}$. Of course, the special hierarchy $m_\sigma < m_\chi \ll \Lambda_{\text{FN}}$ may be contrived if $\lambda_s \ll 1$, but we do not pursue this possibility since we expect the region of viability to be small for light σ in the face of flavor constraints. Also, as we mentioned in the Introduction, we wish to keep the introduction of new mass scales minimal (violated in this case by the introduction of m_χ).

To summarize, $U(1)_{\text{FN}}$ -neutral DM can possibly lead to successful freeze-out through p -wave annihilations to σ pairs, but only a small region would survive flavor constraints. A larger region of viability is possible if DM can annihilate to $\sigma + \rho$ through the s -wave instead. In the next sub-section we will show that DM charged under $U(1)_{\text{FN}}$ is more successful in this respect.

III.1.2. $U(1)_{\text{FN}}$ -charged DM

DM charged under $U(1)_{\text{FN}}$ must acquire its mass, and interactions with the flavon quanta s , via symmetry-breaking. Specifically, DM acquires a Dirac mass and

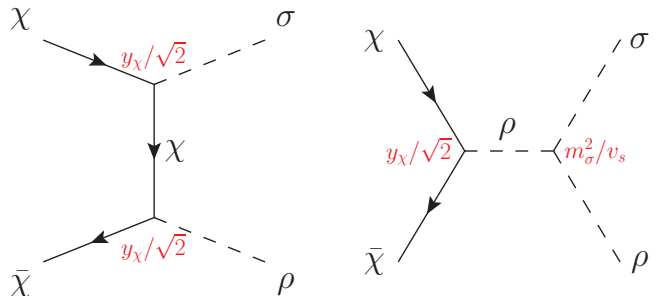


Figure 1. Feynman diagrams contributing to the s -wave annihilation of DM to a CP-even + CP-odd flavon. When kinematically allowed, this channel dominates for DM charged $1/2$ under $U(1)_{\text{FN}}$. See text for more details.

couplings to S through the operator

$$y_\chi \left(\frac{S}{\Lambda_{\text{FN}}} \right)^n S\chi_a\chi_b, \quad (6)$$

given by

$$m_\chi = \frac{y_\chi}{\sqrt{2}} v_s \epsilon^n, \quad g_{s\chi\chi} = (n+1) \frac{y_\chi}{\sqrt{2}} \epsilon^n, \quad (7)$$

where n determines $\mathcal{Q}_\chi \equiv$ the collective charge of χ_a and χ_b as

$$\mathcal{Q}_\chi = (n+1)/2.$$

Without loss of generality, we take y_χ to be real. The only free parameters in this set-up are now

$$\begin{aligned} \text{Scales} &: \Lambda_{\text{FN}}, b^2, \\ \text{Charge} &: \mathcal{Q}_\chi, \\ \text{Couplings} &: y_\chi, \lambda_s, \lambda_{sh}. \end{aligned} \quad (8)$$

It is among these parameters that we must find successful freezeout conditions and identify the relic surface. For our phenomenological treatment in Sec. IV, we neglect λ_{sh} , for it plays little role in our freezeout: as we will show in Sec. III.2, its influence by means of turning on a small Higgs- σ mixing is negligible.

We now proceed to find our desired conditions. First, we notice that Eq. 7 allows for the s -wave process $\chi\bar{\chi} \rightarrow \sigma\rho$. Both the s - and t -channel diagrams in Fig. 1 contribute, and lead to the annihilation cross section given in Appendix B. For $m_\rho \ll m_\chi$, this is schematically

$$\begin{aligned} \langle\sigma v\rangle &\sim \frac{1}{s} |\mathcal{M}|^2 \sim \frac{1}{4m_\chi^2} f'' \\ &\sim \frac{\epsilon^2}{4\Lambda_{\text{FN}}^2} f', \end{aligned} \quad (9)$$

where f'' and f' are functions of y_χ, λ_s, n and ϵ . The above equation implies our set-up can give us a potential *upper* limit on the Froggatt-Nielsen scale Λ_{FN}

when we require the thermal cross section $\langle\sigma v\rangle_{\text{th}} = 4.4 \times 10^{-26} \text{ cm}^3 \text{ s}^{-1}$. This must happen when we require that the coefficient y_χ be perturbative ($y_\chi \leq 4\pi$). In the following we will derive this upper limit on Λ_{FN} for a few select cases.

Let us begin our investigation of DM annihilations with the case of $n = 0$ ($\Rightarrow \mathcal{Q}_\chi = 1/2$). Here

$$\begin{aligned} m_\chi &= \frac{y_\chi}{\sqrt{2}} v_s, \quad g_{s\chi\chi} = \frac{y_\chi}{\sqrt{2}} \\ \Rightarrow \langle\sigma v\rangle &\simeq \frac{3}{2048\pi} \frac{y_\chi^2}{v_s^2}, \end{aligned} \quad (10)$$

where in the second line we have used Eq. B2 and set $m_\chi = m_\sigma$ for simplicity. This can certainly lead to successful freezeout, provided v_s is not so large as to make y_χ non-perturbative. This is not a cause for concern, since Eq. 5 implies $y_\chi \geq 1.9$ if we require the correct abundance at $m_\chi \gg m_\rho$. (For $m_\chi \sim m_\rho$, there is no lower bound on y_χ .) Annihilations to $\sigma + \rho$ are kinematically allowed so long as $m_\sigma + m_\rho < 2m_\chi \Rightarrow 2b^2 < (y_\chi - \sqrt{\lambda_s})^2 v_s^2$. Requiring $y_\chi \leq 4\pi$ gives $\Lambda_{\text{FN}} \leq 13.65 \text{ TeV}$, which is allowed by the limit in Eq. 5.

To sum up, we have found our first successful freezeout scenario without contriving a compressed mass spectrum. Our work will chiefly concern this scenario, for reasons that will become apparent when we inspect the effect of increasing n .

As we increase n , Eq. 7 implies that χ gets lighter, reducing the phase space available for annihilation to $\sigma + \rho$. (One may try to recover some phase space by tuning λ_s small and making σ light, but at the cost of tension with kaon mixing constraints.) Thus the p -wave flavon modes ($\sigma\sigma$ and $\rho\rho$) and SM modes gain in importance. Moreover, inserting Eq. 7 into Eq. 9, $\langle\sigma v\rangle \propto y_\chi^2 (n+1)^4 \epsilon^{2n} / \Lambda_{\text{FN}}^2$ in the $\lambda_s \rightarrow 0$ limit, implying that as we increase n , the upper bound on Λ_{FN} from y_χ perturbativity gets stronger. Eventually this upper bound will fall below the lower bound in Eq. 5. For $m_\chi = m_\sigma$, this occurs at $n = 4$, which gives us an important condition for successful freezeout:

$$n \leq 3, \text{ or } \mathcal{Q}_\chi \leq 2.$$

Conditions on the parameters in Eq. 8 that render desired annihilation modes kinematically allowed may be derived in a straightforward manner from Eqs. 4 and 7.

Our next task is to show that, after imposing these conditions and locating our relic surface, our set-up is quite viable in the face of dark matter experiments. To this end, we pick a single scenario for phenomenological study, $\mathcal{Q}_\chi = 1/2$ ($n = 0$). Our choice is motivated by the following reasons.

(1) As we just showed, the $n = 0$ case provides the maximum phase space for the channel $\chi\bar{\chi} \rightarrow \sigma\rho$, allowing

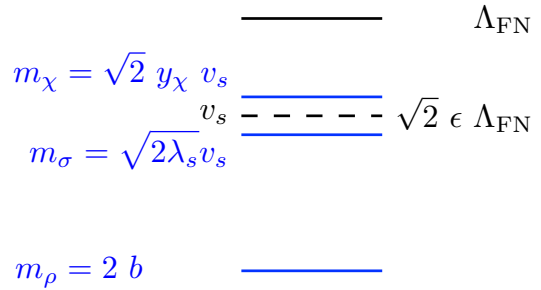


Figure 2. The spectrum studied in this work. The $U(1)_{\text{FN}}$ symmetry breaks at $\sqrt{2}\epsilon$ below the Froggatt-Nielsen scale Λ_{FN} , giving masses to dark matter χ and the CP-even flavon σ at the symmetry-breaking scale v_s . Shown for illustration is a hierarchy in which $m_\chi > m_\sigma$. The mass of the CP-odd flavon ρ , acquired through a freely tunable explicit symmetry breaking parameter b^2 , is assumed $< 2m_\chi - m_\sigma$ in order to allow for DM annihilations to $\rho + \sigma$.

it to dominate the annihilation over a large parametric region. This simplifies the phenomenological analysis.

(2) As Eq. 6 is a marginal operator for $n = 0$, we may relax the assumption that Z_2 -odd vector-like fermions with a common mass Λ_{FN} generate DM-flavon interactions at low energies, and assume no more than the presence of a pair of dark fermions with a combined $U(1)_{\text{FN}}$ charge of unity⁴.

The spectrum of scales in our scenario is sketched in Fig. 2. In general m_χ, v_s and m_σ reside at a common $\mathcal{O}(\text{TeV})$ scale, while m_ρ , a free parameter, can be much lower. The relation between these masses and scales will play a decisive role in our phenomenology.

III.2. Flavon mode domination: an illustration

In the Introduction we had estimated that DM annihilations to all SM final states will be suppressed. We had also surmised that freezeout will be dictated by s -wave annihilations to flavon quanta. In the previous subsection, after identifying $U(1)_{\text{FN}}$ -charged DM as a workable scenario, we derived freezeout conditions ignoring SM modes and including only flavon modes. We now demonstrate the accuracy of our assumptions by quantifying these estimates, which form the crux of our paper.

⁴ We also assume that neither individual charge $\mathcal{Q}_\chi^a, \mathcal{Q}_\chi^b$ is zero. If one of the χ_i is $U(1)_{\text{FN}}$ -neutral, a Majorana mass $\frac{1}{2} M m \chi_i \chi_i$ and the operator $|S|^2 |\chi_i \chi_i| / \Lambda_{\text{FN}}$ are allowed, confounding the freezeout analysis and potentially introducing physical complex phases.

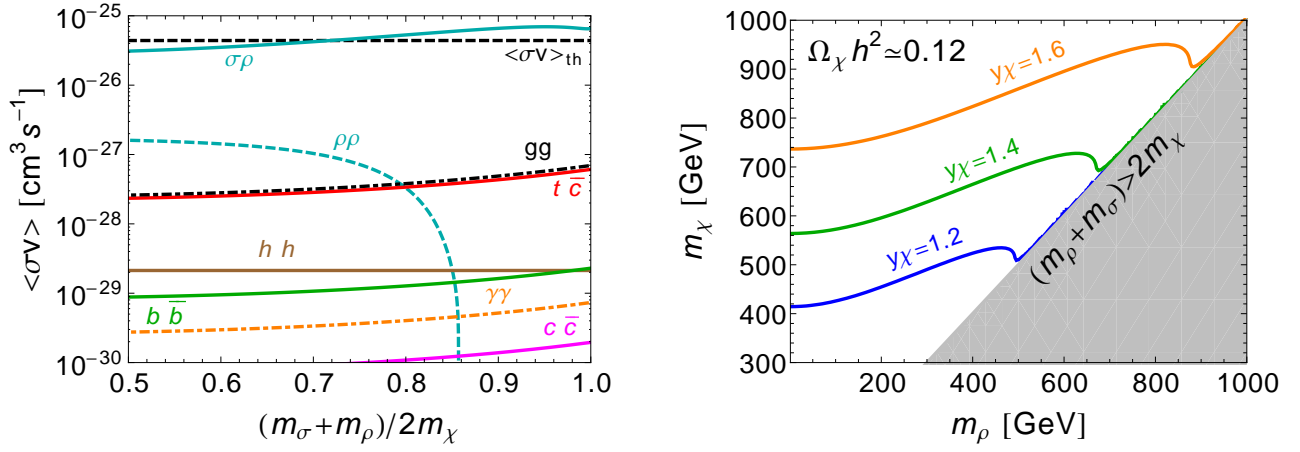


Figure 3. **Left:** Cross sections of various DM annihilation channels as a function of $(m_\sigma + m_\rho)/2m_\chi$, keeping $m_\chi = 950$ GeV, $y_\chi = 1.4$, $\lambda_s = 0.25$, and $\lambda_{sh} = 0.1$. Annihilations to the CP-even σ + CP-odd ρ are seen to dominate over all other modes. **Right:** Contours of y_χ resulting in the correct relic abundance, fixing $m_\sigma = m_\chi$. See text for more details.

The left panel of Fig. 3 shows the $\langle\sigma v\rangle$ of various annihilation modes against the ratio $(m_\rho + m_\sigma)/2m_\chi$, with the thermal cross section $\langle\sigma v\rangle_{\text{th}} = 4.4 \times 10^{-26} \text{ cm}^3 \text{ s}^{-1}$ shown for reference. We have chosen $m_\chi = 950$ GeV, $y_\chi = 1.4$, $\lambda_s = 0.25$ and $\lambda_{sh} = 0.1$ for illustration; this puts m_σ at 678 GeV. The relevant SM modes, hh , $t\bar{c}$, $b\bar{b}$, $c\bar{c}$, gg , and $\gamma\gamma$ are plotted in brown, red, green, magenta, dot-dashed black, and dot-dashed orange respectively, the flavon modes $\sigma\rho$ and $\rho\rho$ in solid blue and dashed blue. Our parametric range kinematically forbids the $\sigma\sigma$ mode, but allowing it does not change our conclusions. We checked our calculations against MicrOmegas 4.3 [40] and found very good agreement.

Let us begin our task by first inspecting the SM final states. Annihilations to Higgs bosons ($\chi\bar{\chi} \rightarrow \sigma^* \rightarrow hh$) proceed through the λ_{sh} vertex in Eq. 3, and suppressed by the twofold effect of its p -wave nature and the large mass of σ in the propagator. This is why the cross section is three orders of magnitude below $\langle\sigma v\rangle_{\text{th}}$. Even for λ_{sh} as large as 1, the above effects would keep the cross section at a factor of 100 below the $\langle\sigma v\rangle_{\text{th}}$. In general, turning on the coupling λ_{sh} would induce h - σ mixing, introducing potential constraints from LHC Higgs measurements. However, due to the hierarchy between the mass scales $m_h \sim v$ and $m_\sigma \sim v_s$, the mixing angle comes out to be $\lesssim 0.1$, which is safe from these constraints. For this reason, and because λ_{sh} plays no role in the freezeout, we consistently neglect it throughout the rest of the paper. As a consequence, we will also not be concerned with (p -wave suppressed) annihilations to the electroweak bosons that would have been prompted by a non-zero λ_{sh} .

Annihilations to SM fermions are highly suppressed as well. These must proceed through flavon mediation in

the s -channel; since both ρ and σ couple to fermion pairs through the Higgs doublet (as seen in Eq. 2), a factor of $(v/\Lambda_{\text{FN}})^2 < 10^{-2}$ appears in the cross section. The relative contributions of the fermion modes is determined by the number of ϵ powers in the DM-flavon coupling, which is shown in Appendix A. Re-writing Eq. A4 (up to $\mathcal{O}(1)$ coefficients) as

$$g_s^u = \frac{1}{v_s} \begin{pmatrix} 8m_u & \epsilon m_c & \epsilon^3 m_t \\ \epsilon^3 m_c & 4m_c & \epsilon^2 m_t \\ \epsilon^5 m_t & \epsilon^2 m_t & 0 \end{pmatrix},$$

$$g_s^d = \frac{1}{v_s} \begin{pmatrix} 7m_d & \epsilon m_s & \epsilon^3 m_b \\ \epsilon m_s & 5m_s & \epsilon^2 m_b \\ \epsilon m_b & \epsilon^2 m_b & 3m_b \end{pmatrix}, \quad (11)$$

we see that except for $t\bar{c}$, $b\bar{b}$ and $c\bar{c}$, all other fermion modes are too feeble.

The presence of a global $U(1)_{\text{FN}}$ anomaly in our set-up gives rise to the annihilation modes $\chi\bar{\chi} \rightarrow \rho^* \rightarrow gg, \gamma\gamma$. Calculating the ρgg and $\rho\gamma\gamma$ couplings using the color and electromagnetic anomaly coefficients that originate from quark triangle diagrams [41], we find the gg cross section comparable to $t\bar{c}$, and the $\gamma\gamma$ cross section 100 times smaller.

We are now left with annihilations to two flavons. The $\sigma\rho$ mode, contributing $> 95\%$ to the total cross section, is dominantly s -wave (with the p -wave contribution so negligible as to vary the solid blue curve only minutely). As advertised in Sec. III.1.2, this annihilation can proceed through an $\mathcal{O}(1)$ -sized coupling to produce $\langle\sigma v\rangle_{\text{th}} = 4.4 \times 10^{-26} \text{ cm}^3 \text{ s}^{-1}$. We see this clearly in the solid blue curve. The $\rho\rho$ (and $\sigma\sigma$) mode is p -wave. Consequently, its cross section is suppressed by about an order of magnitude with respect to the $\sigma\rho$ mode. The cross

section also drops sharply as m_ρ approaches $2m_\chi - m_\sigma$ and shrinks the phase space open for annihilation.

Finally, the right panel of Fig. 3 shows, in the m_ρ - m_χ plane, contours of y_χ that result in successful freezeout. We have set $m_\sigma = m_\chi$ in this plot, which from Eqs. 4 and 10 implies $\lambda_s = y_\chi^2/4$ along each contour. As m_ρ is raised, the phase space available for $\chi\bar{\chi} \rightarrow \sigma\rho$ is reduced, requiring a slight increase in $m_\chi = m_\sigma$ to recover the thermal cross section. One also observes that larger couplings are needed for heavier DM to overcome the m_χ^{-2} suppression of the annihilation cross section.

In the next section we explore the various signals and constraints of our set-up, and show that our parameter space on the relic surface is by and large allowed by flavor and dark matter experiments. Searches best suited for finding our scenario are also identified and discussed.

IV. PHENOMENOLOGY

Since our DM gets its relic abundance effectively by annihilating to mediators, it is a “secluded WIMP” [8], generally hidden from the Standard Model and hence expected to be probed poorly by direct detection and colliders. And though our annihilation is s -wave, allowing our set-up to submit to indirect detection searches, our DM is generally too heavy to produce sufficient photonic flux to be seen. However, flavor-changing processes can competently probe the mediators ρ and σ .

In this section we will discuss the constraints on our scenario from these various experiments, and predict our future prospects. We will begin with flavor experiments, recasting the findings of Ref. [2] in our parameters and finding bounds on m_χ and m_ρ . The most stringent limits here are from kaon mixing measurements. Next we discuss constraints from direct detection, and show that future searches would reach regions that are allowed by kaon mixing. Then we briefly discuss the poor (current and future) sensitivity of indirect detection. Finally, we show that current LHC limits too are weak, and explore promising DM signatures for Run 2.

IV.1. Meson mixing

Both the CP-even σ and CP-odd ρ exhibit flavor violating couplings at tree level (Eq. 11), generating FCNCs and incurring low-energy constraints from meson mixing in neutral K, B and D systems [2]. The strongest limits come from kaon mixing since the SM contribution is rendered small by the GIM mechanism, i.e. it is both loop- and CKM-suppressed. The CP-violation parameter ϵ_K is dominated by short-distance contributions that can be

accurately calculated, whereas the observable Δm_K suffers from a large theoretical uncertainty due to unknown long-distance contributions. For this reason ϵ_K is generally expected to provide the best constraints. Ref. [2] recast results from the **UTfit** collaboration [42] onto the m_ρ - v_s plane, and showed that this is indeed true. Their choice of $\mathcal{O}(1)$ coefficients and $\mathcal{O}(1)$ phases that appear in the Yukawa textures of Eq. A2 does play a role in this result, but one must, for the reasons explained above, expect ϵ_K to outconstrain the CP-preserving Δm_K for most Yukawa textures⁵. We use this result to show our constraints in the m_ρ - m_χ plane in the left panel of Fig. 5, taking advantage of the relation between m_χ, y_χ and v_s in Eq. 10. However, the reader must keep in mind that the limits discussed in the following, as well as the limit quoted in Eq. 5, may be weakened for some choices of the $\mathcal{O}(1)$ coefficients and phases in the Yukawa couplings.

We fix $y_\chi = 2.2$ in Fig. 5 and show with a dashed curve a contour of $\Omega_\chi h^2 = 0.12$. In the regions above this contour, DM is overabundant for this y_χ . The effect of varying this coupling is seen in Fig. 3, however, it must be remembered that raising or lowering y_χ would correspondingly tighten or loosen the ϵ_K bound on m_χ .

The dark shaded region is excluded at 95% C.L. by the ϵ_K measurement, with an illustrative λ_s value of 0.25. As explained in Sec. II, the bound comes from tree-level contributions to $\Delta F = 2$ operator Wilson coefficients, which depend on m_ρ and m_σ . For $m_\rho > 200$ GeV, these contributions scale as $\lambda_s^{-1} v_s^{-4} \propto \lambda_s^{-1} (y_\chi/m_\chi)^4$, hence giving a flat bound across m_ρ . It will prove useful to recast this as a scaling of the lower bound on m_χ in terms of the couplings:

$$m_\chi|_{\epsilon_K} \propto \frac{y_\chi}{\lambda_s^{1/4}}. \quad (12)$$

For $m_\rho < 200$ GeV $\ll m_\sigma$, the flavon contributions to the Wilson coefficients scale as $(v_s m_\rho)^{-2} \propto (m_\chi m_\rho / y_\chi)^{-2}$, giving a bound on m_ρ that falls inversely with m_χ . The dip feature seen between these two regions comes from an accidental cancellation in the Wilson coefficient at $m_\sigma = m_\rho$ due to destructive interference.

This plot illustrates clearly that regions favored by our freezeout scenario are quite viable vis-à-vis flavor constraints. The choice of 2.2 is the smallest y_χ that allows our scenario to escape the ϵ_K bound for all $m_\rho > 200$ GeV. We find that for $1.2 \leq y_\chi \leq 2.2$, our set-up is viable when the relic contour is trapped in the dip feature. For $y_\chi < 1.2$, we are completely excluded.

⁵ We thank F. Bishara (M. Bauer) for raising (clarifying) this point.

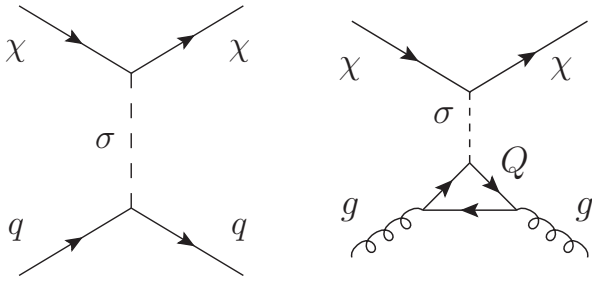


Figure 4. Diagrams contributing to spin-independent scattering with nucleons. Here $q = u, d, s$ and $Q = c, b, t$.

Since regions where our relic contours are excluded mostly correspond to $m_\rho > 200$ GeV, where the scaling in Eq. 12 roughly applies, for our discussions below we will use this equation for making comparisons with constraints from DM experiments. In the following subsections we will pay particular attention to whether these experiments have future sensitivities to parametric regions not excluded by flavor probes.

IV.2. Direct detection

DM can scatter with nucleons through flavon exchange, potentially introducing constraints from direct detection searches. It is well-known that fermion DM scattering with nucleons via pseudoscalar mediator exchange produces a spin-dependent cross section that is velocity-suppressed [43]. Thus, only the exchange of the CP-even σ is relevant to our scenario. As sketched in Fig. 4, this leads to scattering via light quark operators at the tree level and via gluon operators through heavy quark loops. In general, we expect the rates to be small since they will be suppressed by a large m_σ ($\sim v_s$).

Setting aside considerations of relic density for the moment, we now inspect the constraints. We computed our spin-independent cross section σ_{SI} using the formulae in Appendix B. From Eqs. 7, 11 and B3, this cross section scales as

$$\sigma_{\text{SI}} \propto \mu_{\chi N}^2 m_p^2 \left(\frac{y_\chi^8}{\lambda_s^2 m_\chi^6} \right). \quad (13)$$

The right panel of Fig. 5 plots σ_{SI} against m_χ for three choices of y_χ : 1.0 (red), 1.4 (blue) and 2.2 (green), and fixing λ_s to 0.25. The y_χ^8 scaling may be seen by comparing among these curves at some m_χ . The 90% C.L. exclusion cross sections (with their 1 and 2 σ bands) set by Xenon1T [44] are provided for reference. Due to the scaling in Eq. 13, our limit tightens with y_χ . In general, we expect direct detection to constrain the DM mass poorer

than kaon mixing. For instance, one may read off the plot that for $y_\chi = 2.2$, $m_\chi \gtrsim 960$ GeV. This is a weaker bound than the kaon mixing one, illustrated by the pink star at the corresponding m_χ in both the left and right panels of Fig. 5. Variations in y_χ will not change this behavior. Since the exclusion cross section rises only gently across m_χ in this region, we expect from Eq. 13 that the limit on m_χ scales as $y_\chi^{4/3}$. On the other hand, from Eq. 12, we know that the kaon mixing m_χ bound scales as y_χ , which is not much slower than the direct detection scaling.

Our future direct detection prospects are quite interesting. To check these, we compare our σ_{SI} with the projected reaches of the LUX-ZEPLIN (LZ) [45] and DARWIN [46] experiments, provided in the figure. For $y_\chi = \{1.0, 1.4, 2.2\}$, LZ is sensitive to $m_\chi \lesssim \{0.7, 1.0, 1.6\}$ TeV and DARWIN to $m_\chi \lesssim \{0.8, 1.2, 2.1\}$ TeV. Amusingly, there emerge three distinctive future prospects of our relic surface for the three y_χ choices. We show this by placing a cloverleaf on our σ_{SI} curves for each y_χ at the m_χ that gives $\Omega_\chi h^2 = 0.12$ (the part of the σ_{SI} curve to the left/right of the cloverleaf corresponds to DM freezing out under/over-abundantly. Also, as seen in the left panel of Fig. 5, the relic contour is near-insensitive to m_ρ , and mostly picked by m_χ). By scanning the cloverleaves (at $m_\chi \simeq \{0.55, 1.1, 2.7\}$ TeV) and the points where our σ_{SI} curves intersect with LZ and DARWIN, we conclude that

- (a) both LZ and DARWIN can reach $y_\chi = 1.0$,
- (b) LZ cannot, but DARWIN can, reach $y_\chi = 1.4$,
- (c) neither LZ nor DARWIN can reach $y_\chi = 2.2$.

As we had mentioned in the previous sub-section, for $y_\chi \in [1.2, 2.2]$ our relic contour evades the ϵ_K bound in the dip feature. Thus we have a small range of y_χ that gives the correct abundance, is currently viable with respect to all constraints, and is discoverable by future direct detection searches. (Note that although $y_\chi > 2.2$ evades the ϵ_K bound even without help from the dip feature, it is not discoverable at direct detection.) Though these results were obtained after fixing λ_s , varying it would not change the broad conclusions.

We end this sub-section on a final note. Throughout the above, we have set $\lambda_{sh} = 0$ following the motivation in Sec. III.2, but had we turned it on and enabled mixing with the Higgs boson, some contribution to scattering cross sections due to Higgs and gauge boson exchange may have arisen; however, these are completely negligible due to the small mixing angles quoted in Sec. III.2.

IV.3. Indirect detection

Fermi-LAT observations of gamma rays from stacked dwarf galaxies [47] have set 90% C.L. limits on DM anni-

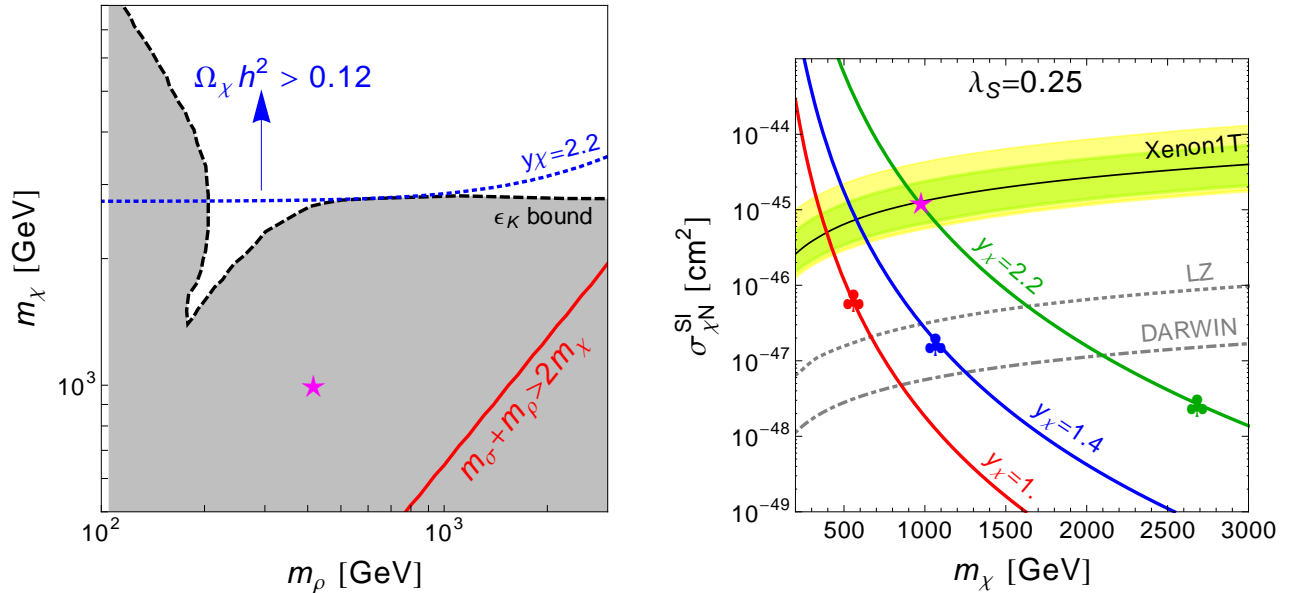


Figure 5. **Left:** 95% C.L. bounds from ϵ_K measurements (dark shaded region excluded) in the m_χ - m_ρ plane, at $\lambda_s = 0.25$ and $y_\chi = 2.2$. The blue dashed curve is a contour of $\Omega_\chi h^2 = 0.12$; the region above it leads to overabundant DM. The region to the right of the red line is kinematically forbidden. **Right:** Spin-independent DM-nucleon scattering cross sections as a function of m_χ for $y_\chi = 1.0, 1.4$ and 2.2 (red, green, and blue curves), versus current constraints from Xenon1T (solid black) and future sensitivities at LZ and DARWIN (dotted and dot-dashed). The cloverleaf on each y_χ curve shows the m_χ that leads to $\Omega_\chi h^2 = 0.12$. **Both panels:** The pink star in the right-hand panel at $m_\chi = 960$ GeV is replicated at the same mass in the left-hand panel – this is as an example indication that regions excluded by direct detection are usually even more deeply excluded by kaon mixing constraints.

hilation cross sections that can reach $\langle\sigma v\rangle_{\text{th}} = (\eta) 2.2 \times 10^{-26} \text{ cm}^3 \text{ s}^{-1}$, potentially affecting our set-up since our annihilation $\chi\bar{\chi} \rightarrow \sigma\rho$ is mainly s -wave. However, these limits are generally much weaker than the ϵ_K bound discussed in Sec. IV.1. Consider the strongest Fermi-LAT bound, that from a 100% $b\bar{b}$ final state: for $\langle\sigma v\rangle = \langle\sigma v\rangle_{\text{th}}$, DM mass $\gtrsim 100$ GeV. Although our annihilation scenario is different – SM final states are products of σ and ρ decay, i.e. we have cascaded, as opposed to direct, annihilations – the corresponding limit on m_χ must not be too far from 100 GeV. Indeed, we find that $m_\chi \gtrsim 175$ GeV from a naive recasting that assumes (a) the integrated photon flux from our DM cascaded annihilation equals that from direct annihilation to $b\bar{b}$, (b) equal masses, and hence decay branching ratios, for σ and ρ . This limit falls well short of the one corresponding to the smallest m_χ spared by the ϵ_K bound: $m_\chi \gtrsim 760$ GeV, which occurs at $y_\chi = 1.2$ as explained in Secs. IV.1 and IV.2. Future indirect detection prospects too are dim. By recasting the sensitivities provided in [48], we find that only $m_\chi \lesssim 325$ GeV is within Fermi-LAT’s reach.

These conclusions, based on order-of-magnitude estimates, would hold against variations in λ_s . But they would change dramatically if we choose $n > 0$ ($\mathcal{Q}_\chi > 1/2$)

in Eq. 6, since Eq. 7 implies m_χ can now be lighter and hence in the range of Fermi-LAT. This warrants a thorough investigation of the indirect detection phenomenology of our $n > 0$ parametric families, which we undertake in [14].

IV.4. LHC

The 13 TeV LHC can potentially probe our scenario. The collider prospects of ρ have already been thoroughly explored in Ref. [2]. To summarize these briefly:

- the collider phenomenology primarily arises from the fact that ρ couples strongest to bottom-bottom and top-charm; this can be seen in Eq. (11).
- the production rates are dominated by some combination of $b\bar{b} \rightarrow \rho$, $g b \rightarrow b\rho$ and $g c \rightarrow t\rho$, depending on m_ρ ,
- the decay branching ratios of $\rho \rightarrow b\bar{b}$ and $\rho \rightarrow t\bar{c}$ dominate,
- at a 100 TeV collider, studies of $\text{top} \rightarrow \rho + \text{charm}$ can exclude the region $m_\rho \leq 175$ GeV, whereas

$\sigma(gc \rightarrow t\rho) \times \text{BR}(\rho \rightarrow tc)$ can exclude $175 \text{ GeV} \leq m_\rho \leq 1000 \text{ GeV}$ for $v_s \lesssim 1 \text{ TeV}$.

In the following we focus on the LHC and study additional signals – *our smoking guns* – generated by our introduction of DM. Since we use Ref. [2]’s Yukawa texture, and since generally $\{m_\rho, m_\sigma\} < 2m_\chi$, the branching fractions of the flavon quanta remain the same, and we wish to clarify that adding our DM does not *alter* the phenomenology of [2], only *augment* it.

Using the fact that our DM must be detected as missing energy (in association with a visible particle) and that our mediator couples strongest to $b\bar{b}$ and $t\bar{c}$, we will show that searches for heavy quarks + \cancel{E}_T (mono-bottom and mono-top), as well as monojet searches, are our best strategy. In general, we expect these signals to be difficult to observe. We may see this from two considerations: (1) Being Z_2 -odd, χ must be pair-produced, either through σ production followed by its invisible decay or through an off-shell ρ . The former is kinematically suppressed since $m_\sigma \simeq v_s$ is heavy, the latter phase-space suppressed, (2) In most of our signals, the initial state involves the sea quarks b and c that have low PDFs.

It is for the above reasons that we expect to be quite safe from current bounds, as we will show explicitly at the end of this sub-section. Due to this lack of constraints, we will restrict ourselves in the following to only a qualitative discussion of our best-case signals. A more thorough treatment involving careful background estimates and signal-enriching techniques will be dealt in forthcoming work [14]. For now, we quote generator-level cross sections at $\sqrt{s} = 13 \text{ TeV}$ for a point that evades our stringent kaon mixing constraints, $m_\chi = 760 \text{ GeV}$, $y_\chi = 1.2$, $m_\rho = 175 \text{ GeV}$, $m_\sigma = 315 \text{ GeV}$. These cross sections are monojet: 2.2 ab, mono-bottom: 0.4 ab, mono-top: 0.02 ab.

While below we present our LHC signals with DM production through off-shell ρ , it must be kept in mind that contributions from processes mediated by a possibly light σ may also be relevant.

Monojets

Missing transverse energy accompanied by a single jet is a popular channel for LHC DM searches [49, 50]. This signal arises in our set-up from the diagrams in Fig. 6. Contributions of the form $q\bar{q} \rightarrow \rho^*j$ and those involving lighter quarks in the loop will be negligible because of the weaker couplings. The main backgrounds are $Z(\nu\bar{\nu}) + j$, $W(\nu\ell)$ (ℓ fakes a jet), $W(\nu\ell) + j$ (ℓ is missed). Another significant but poorly understood background comes from QCD jet mismeasurement, usually minimized by a tight \cancel{E}_T cut.

Mono-b

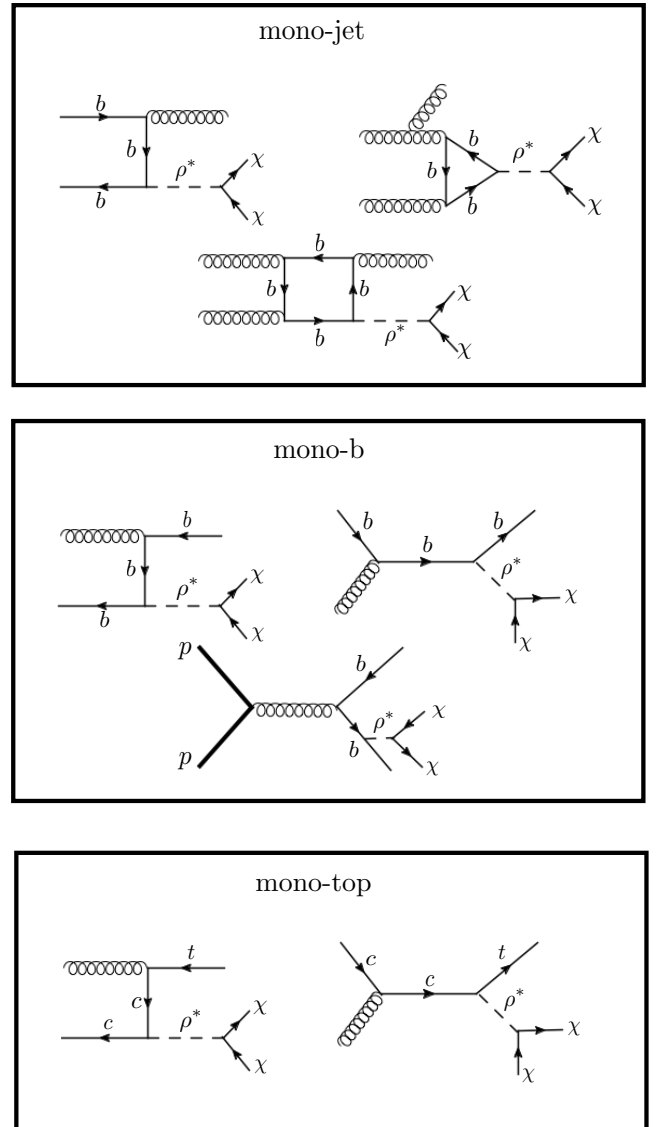


Figure 6. Our main signal processes producing mono-jet, mono-b and mono-top signatures. See text for details on backgrounds and signal-enrichment.

$bg \rightarrow \rho^*b$ (Fig. 6) can contribute to a mono-bottom signal, with subdominant contributions from the flavor-changing processes $qg \rightarrow \rho^*b$, where $q = d, s^6$; $b\bar{b}\rho^*$ production may also contribute when one of the b ’s is missed.

The dominant SM backgrounds are still $Z(\nu\bar{\nu})/W(\nu\ell) + j/c$, where the ordinary or c -tagged jet is misidentified as a b and the ℓ is missed. These contributions, though appearing to be suppressed by mistag

⁶ Although light quarks in the initial state will enhance the cross section due to their PDFs, the coupling of ρ to light quarks is so small that these contributions are sub-dominant to $bg \rightarrow \rho^*b$.

rates, outdo direct b production [51]: $gb \rightarrow bZ(\nu\bar{\nu})$ is the only irreducible background, and just like the signal process $bg \rightarrow \rho^*b$, is PDF suppressed. Future improvements in b -tagging algorithms may reduce the $Z/W + j/c$ background, and cutting high on E_T would help suppress all the backgrounds.

Mono-top

The flavor off-diagonal coupling g_{tc} is comparable in size to g_{bb} (see Eq. (A3)) and helps in obtaining a large signal of mono-tops [52]. See Fig. 6 for the attendant diagrams. With the charm PDF higher than the bottom, this channel may be more relevant than mono- b .

Hadronically decaying tops may be particularly advantageous, since the branching ratio is high (=68%) and since the top mass may be reconstructed from visible final states, aiding in background reduction. The main background is QCD multijets with mismeasured jets, which can be controlled with a high E_T requirement. This may boost the top quark and give near-collinear final products. Hence, instead of three distinct jets, the top may be detected as a single fat jet. All this makes our mono-top similar to our mono-jet (in both signal and backgrounds), except here we further demand $m_{\text{fat jet}} \simeq m_t$ and b -tagging.

Having detailed our signals, we now show the safety of our scenario from constraints at the 8 TeV LHC. Ref. [53] places these bounds for monojet signals on an effective cutoff Λ that mediates χ - q interactions ($q = u, d, s, c, b$), which can be recast to our scenario by mapping our parameters to the definition of Λ . First, we choose the smallest DM mass spared by kaon mixing: 760 GeV (see the previous two sub-sections). If $m_\sigma \sim m_\chi$ and $m_\rho < m_\chi$ (as is true in most regions on our relic surface), the propagator is dominated by the momentum required to pair-produce DM, $2m_\chi$, which is then our cutoff. Thus $\Lambda = 1520$ GeV for both σ -mediated and ρ -mediated DM production. However, Ref. [53] finds the tightest bound to only be $\Lambda > 50$ GeV. Similarly, we can recast the mono- b bound in Ref. [51], which is even weaker: $\Lambda > 90$ GeV. Finally, mono-top signals studied in Ref. [54] set bounds on a model analogous to ours. While our $(g_s)_{tc}$ at the parametric point considered above is 0.01, Ref. [54]’s upper limit on the coupling of a pseudoscalar mediator to the up and top quark $\sim O(1)$. Our actual limit is much weaker, since our ρ and σ production must proceed through the sea charm quark in the initial state as opposed to the valence up quark in Ref. [54], and also because our production rates are hurt by a 3-body final state when ρ is in the propagator. Analogous to our indirect detection limits, our collider limits are generally weaker than flavor limits because $m_\chi \sim v_s$. Again similar to indirect detection, we expect the LHC to probe our scenario better at $n > 0$ since $m_\chi \propto \epsilon^n v_s$ (Eq. 7).

Though we have only considered mono-X searches, other signals involving $\rho^* \rightarrow \chi\bar{\chi}$ may be explored. E.g. a $b\bar{b} + E_T$ signal can arise via QCD b -pair production with one of the b ’s radiating a $\rho^* \rightarrow \chi\bar{\chi}$. The lack of PDF suppression may bolster the signal, but the background also becomes more significant. Moreover, the signal rate falls away for heavy DM. These various tensions make this avenue a potentially interesting study.

V. CONCLUSIONS

In this paper, we investigated the conditions under which fermionic dark matter embedded in the Froggatt-Nielsen mechanism, with a cutoff scale of Λ_{FN} , can freeze out to give the observed abundance. Annihilations to SM species are suppressed by the cutoff scale, while those to the flavon quanta can proceed with $O(1)$ couplings. If neutral under $U(1)_{\text{FN}}$, DM can undergo p -wave-suppressed annihilations to pairs of the CP-even flavon σ , provided a compressed spectrum is contrived. If charged under $U(1)_{\text{FN}}$, DM can annihilate freely to a CP-odd flavon ρ + CP-even flavon σ in the s -wave, as the hierarchy $m_\rho \ll m_\chi$ can be naturally arranged. Flavor constraints on the FN vev v_s and perturbativity of the DM-flavon coupling y_χ together restrict the collective $U(1)_{\text{FN}}$ charge of DM to $\mathcal{Q}_\chi \leq 2$. Perturbativity also sets upper limits on the FN cutoff Λ_{FN} , implying that future experiments sensitive to this scale (such as precision low-energy measurements or a 100 TeV collider) may be able to falsify our scenarios.

We focused on the case of $\mathcal{Q}_\chi = 1/2$, which is viable over a larger parametric region than the cases of higher \mathcal{Q}_χ . We found that while direct detection, indirect detection and LHC searches provide weak constraints, measurements of the CP-violation parameter ϵ_K in kaon mixing probe this scenario well. Future direct detection searches can unearth regions allowed by kaon mixing, but future indirect detection searches cannot. We also discussed possible DM signatures at LHC Run-2 and strategies for enriching the signal over background. The clearest signal of our hypothesis would be a triple discovery of the pseudoscalar flavon, CP-even flavon and DM on the “relic surface” of our parameters, such as along the contours shown in the right panel of Fig. 3. These possibilities will be explored in greater detail in a forthcoming paper [14]. In it we will more closely examine the implications of indirect detection on the entire parameter space in Eq. 7, studying each \mathcal{Q}_χ scenario in detail. We will also undertake a fuller collider study of our LHC signals.

Our set-up can be trivially extended to include the leptonic FN mechanism, in which case future AMS-02 measurements could become relevant. Gauging the $U(1)_{\text{FN}}$

symmetry is another possibility, potentially introducing Z' bosons as a DM annihilation channel, and as an avenue for a new set of constraints. Spin-0 DM takes our analysis into non-trivial directions, since by virtue of the Higgs portal term $|\chi|^2|H|^2$, annihilations could now be shared amongst flavon- and Higgs-pair channels. We leave all these possibilities for future study.

In summary, it is intriguing that thermal freezeout provides a target for exploring not only the identity of dark matter but also the apparatus behind flavor.

ACKNOWLEDGMENTS

We are thankful to Fady Bishara for collaboration in the initial stages of this work and for enlightening Skype sessions, to Antonio Delgado for spirited discussions and insights into explicit symmetry breaking and global symmetries, to Wolfgang Altmannshofer, Martin Bauer, Chris Kolda, Adam Martin, Tilman Plehn, Oleg Popov, and Flip Tanedo for conversations, and the anonymous referee for helpful comments. We thank A. Martin and A. Delgado for reading the manuscript. This work was supported by the National Science Foundation under Grants No. PHY-1417118 and No. PHY-1520966.

Appendix A: Yukawa couplings

The quark masses arising from Eq. 2 are

$$(m_u)_{ij} = y_{ij}^{(u)} \epsilon^{\mathcal{Q}_{q_i} - \mathcal{Q}_{u_j}} \frac{v}{\sqrt{2}}, \quad (m_d)_{ij} = y_{ij}^{(d)} \epsilon^{\mathcal{Q}_{q_i} - \mathcal{Q}_{d_j}} \frac{v}{\sqrt{2}}, \quad (\text{A1})$$

with the possibility

$$\begin{pmatrix} \mathcal{Q}_{q_1} & \mathcal{Q}_{q_2} & \mathcal{Q}_{q_3} \\ \mathcal{Q}_u & \mathcal{Q}_c & \mathcal{Q}_t \\ \mathcal{Q}_d & \mathcal{Q}_s & \mathcal{Q}_b \end{pmatrix} = \begin{pmatrix} -3 & -2 & 0 \\ 5 & 2 & 0 \\ 4 & 3 & 3 \end{pmatrix}$$

yielding the correct masses [2].

The corresponding Yukawa interactions with the physical Higgs are identified as $(Y_{ij}^u/\sqrt{2})h\bar{u}_{L_i}u_{R_j}$ and $(Y_{ij}^d/\sqrt{2})h\bar{d}_{L_i}d_{R_j}$ with

$$Y_{ij}^u \equiv y_{ij}^{(u)} \epsilon^{\mathcal{Q}_{q_i} - \mathcal{Q}_{u_j}}, \quad Y_{ij}^d \equiv y_{ij}^{(d)} \epsilon^{\mathcal{Q}_{q_i} - \mathcal{Q}_{d_j}}. \quad (\text{A2})$$

From Eqs. 1 and 2, one also obtains the Yukawa interactions

$$g_{ij}^q \sigma \bar{f}_{L_i} f_{R_j} + g_{ij}^q \gamma_5 \rho \bar{f}_{L_i} f_{R_j} \quad (\text{A3})$$

with

$$(g_\sigma^u)_{ij} = i(g_\rho^u)_{ij} = y_{ij}^{(u)} (\mathcal{Q}_{q_i} - \mathcal{Q}_{u_j}) \epsilon^{(\mathcal{Q}_{q_i} - \mathcal{Q}_{u_j})} \frac{v}{\sqrt{2}v_s},$$

$$(g_\sigma^d)_{ij} = i(g_\rho^d)_{ij} = y_{ij}^{(d)} (\mathcal{Q}_{q_i} - \mathcal{Q}_{d_j}) \epsilon^{(\mathcal{Q}_{q_i} - \mathcal{Q}_{d_j})} \frac{v}{\sqrt{2}v_s}. \quad (\text{A4})$$

The $g_s^{(u,d)}$ matrices are brought to the mass basis via the biunitary transformations that diagonalize the Higgs Yukawas $Y_{ij}^{(u,d)} \equiv y_{ij}^{(u,d)} \epsilon^{n_{ij}(m_{ij})}$. Due to the misalignment between the Higgs and flavon Yukawa bases, the σ and ρ can mediate flavor-violating interactions that may be subject to meson-mixing constraints.

Appendix B: Dark matter formulae

This appendix collects formulae used in the calculation of the relic density and direct detection cross sections.

Relic abundance

The relic abundance is given by [55]

$$\Omega_\chi h^2 = 0.12 \frac{4.4 \times 10^{-26} \text{ cm}^3/\text{s}}{\langle \sigma v \rangle} \left(\frac{x_f}{25} \right) \left(\frac{106}{g_*} \right)^{1/2}, \quad (\text{B1})$$

where $x_f \equiv m_\chi/T_{\text{freezeout}}$ and g_* counts the entropy degrees of freedom at freezeout. The annihilation cross section $\langle \sigma v \rangle$ is dominated by process $\chi\bar{\chi} \rightarrow \sigma\rho$, and its s -wave piece is given by

$$\langle \sigma v \rangle_{s\text{-wave}} = \frac{g_{\rho\chi\chi}^2}{256\pi m_\chi^4 (4m_\chi^2 - m_\rho^2)^2 (4m_\chi^2 - m_\sigma^2 - m_\rho^2)^2} \sqrt{(4m_\chi^2 - m_\sigma^2)^2 - 2m_\rho^2(4m_\chi^2 + m_\sigma^2) + m_\rho^4} \times \left\{ -g_{\sigma\chi\chi} m_\rho^4 + m_\rho^2 (2m_\chi \lambda_{\sigma\rho\rho} + m_\sigma^2 g_{\sigma\chi\chi}) + 2m_\chi (4m_\chi^2 - m_\sigma^2) (2m_\chi g_{\sigma\chi\chi} - \lambda_{\sigma\rho\rho}) \right\}^2, \quad (\text{B2})$$

where the couplings $g_{\rho\chi\chi} = g_{\sigma\chi\chi} = y_\chi/\sqrt{2}$ and $\lambda_{\sigma\rho\rho} = m_\sigma^2/v_s$. As mentioned in Sec. III.2, the p -wave contribution is found negligible.

Direct detection

The spin-independent DM-nucleon scattering cross section is given by [56]

$$\sigma_{\chi N}^{\text{SI}} = \frac{\mu_{\chi N}^2}{\pi} f_N^2, \quad (\text{B3})$$

with $\mu_{\chi N}$ the DM-nucleon reduced mass. The effective nucleon-DM coupling f_N arises from the operators $(\bar{\chi}\chi)(\bar{q}q)$ and $\bar{\chi}\chi\mathcal{G}_{\mu\nu}^a\mathcal{G}^{a\mu\nu}$ (via heavy quark loops), and is given by [57]

$$f_N = m_N \left(\sum_{q=u,d,s} f_q f_{T_q}^N + \sum_{q=c,t,b} \frac{2}{27} f_q f_{T_G}^N c_q \right), \quad (\text{B4})$$

with the mass fractions in nucleons

$$f_{T_{u,d,s}}^p = (0.023, 0.032, 0.020), \quad f_{T_{u,d,s}}^n = (0.017, 0.041, 0.020), \\ f_{T_G}^p = 0.925, \quad f_{T_G}^n = 0.922,$$

and c_q a QCD correction factor $= 1 + 11\alpha_s(m_q)/4\pi$ with $(c_c, c_b, c_t) = (1.32, 1.19, 1)$. The effective quark-DM couplings are given by

$$f_q = \left(\frac{g_{\sigma\chi\chi} g_{\sigma qq}}{m_q m_\sigma^2} \right),$$

with $g_{\sigma\chi\chi} = y_\chi/\sqrt{2}$ and $g_{\sigma qq}$ are the couplings obtained after rotating to the mass basis the couplings given in Eq. A4.

-
- [1] C. D. Froggatt and H. B. Nielsen, Nucl. Phys. B **147**, 277 (1979).
- [2] M. Bauer, T. Schell and T. Plehn, Phys. Rev. D **94**, no. 5, 056003 (2016) [arXiv:1603.06950 [hep-ph]].
- [3] N. Arkani-Hamed, A. Delgado and G. F. Giudice, Nucl. Phys. B **741**, 108 (2006) [hep-ph/0601041].
- [4] J. Bramante, P. J. Fox, A. Martin, B. Ostdiek, T. Plehn, T. Schell and M. Takeuchi, Phys. Rev. D **91**, 054015 (2015) [arXiv:1412.4789 [hep-ph]].
- [5] J. Bramante, N. Desai, P. Fox, A. Martin, B. Ostdiek and T. Plehn, Phys. Rev. D **93**, no. 6, 063525 (2016) [arXiv:1510.03460 [hep-ph]].
- [6] M. Cirelli, N. Fornengo and A. Strumia, Nucl. Phys. B **753**, 178 (2006) [hep-ph/0512090].
- [7] M. Cirelli and A. Strumia, New J. Phys. **11**, 105005 (2009) [arXiv:0903.3381 [hep-ph]].
- [8] M. Pospelov, A. Ritz and M. B. Voloshin, Phys. Lett. B **662**, 53 (2008) [arXiv:0711.4866 [hep-ph]].
- [9] S. Chang, R. Edezhath, J. Hutchinson and M. Luty, Phys. Rev. D **89**, no. 1, 015011 (2014) [arXiv:1307.8120 [hep-ph]].
- [10] S. Chang, R. Edezhath, J. Hutchinson and M. Luty, Phys. Rev. D **90**, no. 1, 015011 (2014) [arXiv:1402.7358 [hep-ph]].
- [11] R. T. D’Agnolo and J. T. Ruderman, arXiv:1505.07107 [hep-ph].
- [12] A. Delgado, A. Martin and N. Raj, Phys. Rev. D **95**, no. 3, 035002 (2017) [arXiv:1608.05345 [hep-ph]].
- [13] B. Batell, M. Pospelov and A. Ritz, Phys. Rev. D **79**, 115019 (2009) [arXiv:0903.3396 [hep-ph]].
- [14] C. Alvarado, F. Elahi, N. Raj (in preparation).
- [15] K. Griest and M. Kamionkowski, Phys. Rev. Lett. **64**, 615 (1990).
- [16] L. Calibbi, A. Crivellin and B. Zaldivar, Phys. Rev. D **92**, no. 1, 016004 (2015) [arXiv:1501.07268 [hep-ph]].
- [17] K. S. Babu and S. Nandi, Phys. Rev. D **62**, 033002 (2000) [hep-ph/9907213].
- [18] G. F. Giudice and O. Lebedev, Phys. Lett. B **665**, 79 (2008) [arXiv:0804.1753 [hep-ph]].
- [19] M. Bauer, M. Carena and K. Gemmler, JHEP **1511**, 016 (2015) [arXiv:1506.01719 [hep-ph]].
- [20] M. Bauer, M. Carena and K. Gemmler, Phys. Rev. D **94**, no. 11, 115030 (2016) [arXiv:1512.03458 [hep-ph]].
- [21] L. Calibbi, Z. Lalak, S. Pokorski and R. Ziegler, JHEP **1207**, 004 (2012) [arXiv:1204.1275 [hep-ph]].
- [22] B. Batell, J. Pradler and M. Spannowsky, JHEP **1108**, 038 (2011) [arXiv:1105.1781 [hep-ph]].
- [23] J. F. Kamenik and C. Smith, JHEP **1203**, 090 (2012) [arXiv:1111.6402 [hep-ph]].
- [24] M. J. Dolan, F. Kahlhoefer, C. McCabe and K. Schmidt-Hoberg, JHEP **1503**, 171 (2015) Erratum: [JHEP **1507**, 103 (2015)] [arXiv:1412.5174 [hep-ph]].
- [25] F. Bishara and J. Zupan, JHEP **1501**, 089 (2015) [arXiv:1408.3852 [hep-ph]].
- [26] J. Kile, Mod. Phys. Lett. A **28**, 1330031 (2013) [arXiv:1308.0584 [hep-ph]].
- [27] J. F. Kamenik and J. Zupan, Phys. Rev. D **84**, 111502 (2011) [arXiv:1107.0623 [hep-ph]].
- [28] I. de Medeiros Varzielas, O. Fischer and V. Maurer, JHEP **1508**, 080 (2015) [arXiv:1504.03955 [hep-ph]].
- [29] F. Bishara, A. Greljo, J. F. Kamenik, E. Stamou and J. Zupan, JHEP **1512**, 130 (2015) [arXiv:1505.03862 [hep-ph]].
- [30] I. de Medeiros Varzielas and O. Fischer, JHEP **1601**, 160 (2016) [arXiv:1512.00869 [hep-ph]].
- [31] I. Galon, A. Kwa and P. Tanedo, JHEP **1703**, 064 (2017) [arXiv:1610.08060 [hep-ph]].
- [32] P. Agrawal, S. Blanchet, Z. Chacko and C. Kilic, Phys. Rev. D **86**, 055002 (2012) [arXiv:1109.3516 [hep-ph]].
- [33] P. Agrawal, M. Blanke and K. Gemmler, JHEP **1410**, 72 (2014) [arXiv:1405.6709 [hep-ph]].
- [34] P. Agrawal, Z. Chacko, E. C. F. S. Fortes and C. Kilic, Phys. Rev. D **93**, no. 10, 103510 (2016) [arXiv:1511.06293 [hep-ph]].
- [35] J. Kile, Mod. Phys. Lett. A **28**, 1330031 (2013) [arXiv:1308.0584 [hep-ph]].
- [36] K. S. Babu, arXiv:0910.2948 [hep-ph].

- [37] W. L. K. Wu, J. Errard, C. Dvorkin, C. L. Kuo, A. T. Lee, P. McDonald, A. Slosar and O. Zahn, *Astrophys. J.* **788**, 138 (2014) [arXiv:1402.4108 [astro-ph.CO]].
- [38] K. N. Abazajian *et al.* [Topical Conveners: K.N. Abazajian, J.E. Carlstrom, A.T. Lee Collaboration], *Astropart. Phys.* **63**, 66 (2015) [arXiv:1309.5383 [astro-ph.CO]].
- [39] J. Errard, S. M. Feeney, H. V. Peiris and A. H. Jaffe, *JCAP* **1603**, no. 03, 052 (2016)
- [40] G. Belanger, F. Boudjema, A. Pukhov and A. Semenov, arXiv:1305.0237 [hep-ph].
- [41] B. Bellazzini, C. Csaki, J. Hubisz, J. Shao and P. Tanedo, *JHEP* **1109**, 035 (2011) [arXiv:1106.2162 [hep-ph]].
- [42] M. Bona *et al.* [UTfit Collaboration], *JHEP* **0803**, 049 (2008) [arXiv:0707.0636 [hep-ph]].
- [43] J. Kumar and D. Marfatia, *Phys. Rev. D* **88**, no. 1, 014035 (2013) [arXiv:1305.1611 [hep-ph]].
- [44] E. Aprile *et al.* [XENON Collaboration], arXiv:1705.06655 [astro-ph.CO].
- [45] D. S. Akerib *et al.* [LZ Collaboration], arXiv:1509.02910 [physics.ins-det].
- [46] J. Aalbers *et al.* [DARWIN Collaboration], *JCAP* **1611**, 017 (2016) [arXiv:1606.07001 [astro-ph.IM]].
- [47] M. Ackermann *et al.* [Fermi-LAT Collaboration], *Phys. Rev. D* **89**, 042001 (2014)
- [48] S. Funk, *Proc. Nat. Acad. Sci.* **112**, 2264 (2015) [arXiv:1310.2695 [astro-ph.HE]].
- [49] G. Aad *et al.* [ATLAS Collaboration], *Eur. Phys. J. C* **75**, no. 7, 299 (2015) Erratum: [*Eur. Phys. J. C* **75**, no. 9, 408 (2015)] [arXiv:1502.01518 [hep-ex]].
- [50] M. Aaboud *et al.* [ATLAS Collaboration], *Phys. Rev. D* **94**, no. 3, 032005 (2016) [arXiv:1604.07773 [hep-ex]].
- [51] T. Lin, E. W. Kolb and L. T. Wang, *Phys. Rev. D* **88**, no. 6, 063510 (2013) [arXiv:1303.6638 [hep-ph]].
- [52] J. Andrea, B. Fuks and F. Maltoni, *Phys. Rev. D* **84**, 074025 (2011) [arXiv:1106.6199 [hep-ph]].
- [53] U. Haisch, F. Kahlhoefer and E. Re, *JHEP* **1312**, 007 (2013) [arXiv:1310.4491 [hep-ph]].
- [54] J. L. Agram, J. Andrea, M. Buttignol, E. Conte and B. Fuks, *Phys. Rev. D* **89**, no. 1, 014028 (2014) [arXiv:1311.6478 [hep-ph]].
- [55] G. Steigman, B. Dasgupta and J. F. Beacom, *Phys. Rev. D* **86**, 023506 (2012) [arXiv:1204.3622 [hep-ph]].
- [56] J. Abdallah *et al.*, *Phys. Dark Univ.* **9-10**, 8 (2015) [arXiv:1506.03116 [hep-ph]].
- [57] J. Hisano, K. Ishiwata and N. Nagata, *Phys. Rev. D* **82**, 115007 (2010) [arXiv:1007.2601 [hep-ph]].